

DOI:10.11835/j.issn.2096-6717.2020.124

开放科学(资源服务)标识码(OSID):



## Enhanced mechanical properties of mortar with graphene in the traditional sandstone cultural relics conservation

QIAO Zhen<sup>1</sup>, WANG Jie<sup>1</sup>, SUN Bo<sup>1,2</sup>, WANG Fengrui<sup>1,2</sup>, DING Zihan<sup>1</sup>, YANG Tianyu<sup>3</sup>

(1. Northwest Research Institute Co. Ltd. of C. R. E. C., Lanzhou 730000, P. R. China; 2. School of Civil Engineering and Mechanics, Lanzhou University, Lanzhou 730000, P. R. China; 3. Leshan Giant Buddha Management Committee, Leshan 614003, Sichuan, P. R. China)

**Abstract:** More than 8 000 grottoes and cliff statues are located in Sichuan and Chongqing. Most are made from sandstone. The sandstone has deteriorated due to long-term environmental effects, posing a threat to the cultural relics. Graphene sheets are added to the traditional mortar of the sandstone cultural relics to enhance the properties, which is defined as “CH@G mortar”. The mechanical properties and volume stability of the CH@G mortar are enhanced by the graphene sheets. The highest strength is obtained by the addition of 0.07% graphene sheets, and its values (increased proportion compared with CH mortar) of compressive strength, flexural strength and tensile strength at 56 d are 4.21 MPa (7.36%), 2.21 MPa (19.46%) and 0.47 MPa (51.61%), respectively. The FT-IR and Raman spectra results show that the graphene sheets have little influence on the composition of the products, and could accelerate the hydration in the early days, according to the XRD results. The SEM images show that graphene sheets could form a uniform and compacted microstructure.

**Keywords:** sandstone cultural relics; mortar; graphene; mechanical properties

## 石墨烯增强传统砂岩文物修复材料性能研究

乔榛<sup>1</sup>, 王捷<sup>1</sup>, 孙博<sup>1,2</sup>, 王逢睿<sup>1,2</sup>, 丁梓涵<sup>1</sup>, 杨天宇<sup>3</sup>

(1. 中铁西北科学研究院有限公司, 兰州 730000; 2. 兰州大学 土木工程与力学学院, 兰州 730000; 3. 乐山大佛风景名胜区管理委员会, 四川 乐山 614003)

**摘要:**川渝地区分布有8 000余处石窟和摩崖造像,大部分凿刻于砂岩中,长期环境作用导致砂岩性能劣化,对赋存文化遗产的安全造成威胁。为了提升传统砂岩文物修复材料的性能,将石墨烯纳米片加入传统修复材料中,运用传统工艺制备出“CH@G”灰浆。结果表明,加入石墨烯纳米片的CH@G灰浆的力学性能和体积稳定性较传统材料明显提高。当石墨烯纳米片的添加量为质量百分比0.07%时,样品力学性能最佳,56 d抗压强度、抗折强度和抗拉强度分别为4.21、2.21、0.47 MPa,相对于传统修复材料,强度分别提升了7.36%、19.46%、51.61%。FT-IR、Raman和XRD结果表明,石墨烯纳米片对固化反应产物影响较小,并且可以在早期加速水化反应,从而提升早期强度。SEM结果表明,石墨烯纳米片作为一种调节相,促使灰浆形成均匀致密的微观结构。

**关键词:**砂岩文物;灰浆;石墨烯;力学性能

**中图分类号:** TU599 **文献标志码:** A **文章编号:** 2096-6717(2021)01-0155-09

Received: 2020-04-07

**Foundation items:** Sichuan Science and Technology Program (No. 2020YFS0391); Key Research Project of China Railway Academy Co. Ltd. (No. 2019-KJ011-Z010-A2, 2020-KJ009-Z009-A2).

**Author brief:** QIAO Zhen (1991-), main research interest: cultural relics heritage conservation, E-mail: 409434721@qq.com.

## 1 Introduction

There are more than 8 000 grottoes and cliff statues located in Sichuan and Chongqing. These are mainly carved out of the thick sandstone and mudstone strata of the Jurassic Period of the Mesozoic Era. The most famous stone cultural relics are the Leshan Giant Buddha and the Dazu rock carvings<sup>[1]</sup>. The sandstone cultural relics have deteriorated over time due to both environmental causes and human activity, and conservation work has been carried out several times in the past decades in an effort to preserve them<sup>[2]</sup>. In 2001, Chinese experts used traditional materials to repair the head, chest and abdomen of the Leshan Giant Buddha.

The mortar used for the conservation of traditional sandstone cultural relics is a cementitious material composed of lime, sand, slag and a small amount of cement. Cementitious materials possess relatively high compressive strength, but lack toughness and volume stability<sup>[3-5]</sup>. The traditional materials used in the chest and abdomen areas of the Leshan Giant Buddha show some deterioration due to multiple factors. The deterioration of the chest and abdomen (exfoliation, hollow, crack and water infiltration) is shown in Fig. 1.

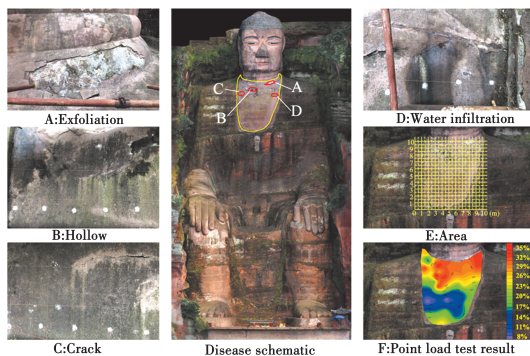


Fig. 1 Schematic images showing deterioration of Leshan Giant Buddha

Graphene, which has a high elastic modulus (1 TPa) and excellent mechanical properties (130 GPa)<sup>[6-10]</sup>, is considered an ideal candidate for improving the mechanical properties of cementitious material, and previous results indicate that adding graphene to cementitious matrices can enhance the toughness of the resultant composites<sup>[11-15]</sup>.

In this paper, traditional mortar used in the conservation of sandstone cultural relics is named CH mortar due to its Chinese name “Chui Hui”. Graphene is used to improve their mechanical properties, and the mortars with graphene are defined as CH@G mortars. Mechanical properties, shrinkage rate, ultrasonic wave velocity, the composition of the products, morphology and the mechanism of the graphene effect are investigated.

## 2 Experimental Section

### 2.1 Materials

#### 2.1.1 CH mortar

The raw materials of the CH mortar were lime, slag, sand and a small amount of cement. Mixing and ramming were employed to make the particles distribute uniformly.

The cement and lime were local products. The X-Ray Diffraction (XRD) results are shown in Table 1. The sand was purchased from Xiamen ISO Standard Sand Co, Ltd.. The slag, which was steel mill waste, was purchased from Desheng Steel Co., Ltd. in Leshan. The particle size distribution curves of the slag and sand are shown in Fig. 2.

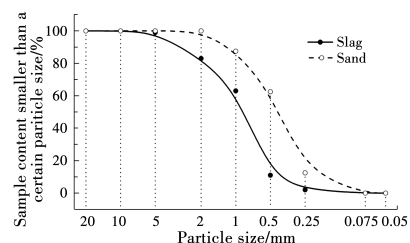


Fig. 2 Particle size distribution curves of slag and sand

Table 1 XRD Semi-quantitative analysis of cement and lime

Raw Material	C <sub>3</sub> S/%	C <sub>2</sub> S/%	C <sub>3</sub> A/%	C <sub>4</sub> AF/%	Raw Material	Ca(OH) <sub>2</sub> /%	CaCO <sub>3</sub> /%	SiO <sub>2</sub> /%
Cement	60.88	18.49	7.22	13.41	Lime	90.70	6.09	3.61

### 2.1.2 Graphene

Graphene sheets were purchased from Deyang Carbonene Co. in Sichuan province. The microstructure and chemical composition were tested by Transmission Electron Microscope (TEM), High Resolution Transmission Electron Microscope (HRTEM) and X-ray Photoelectron Spectroscopy (XPS). As shown in Fig. 3 (a), the microstructure of graphene is similar to overlapping nano-fibers. Fig. 3 (b) shows the HRTEM image of the graphene sheet. The sheet has 6~7 single carbon layers. As shown in Fig. 3 (c), the intensity of the C1s peak is greater than that of the O1s peak. The C1s spectrum contains four peaks, including peak A (C=C) at 284.4 eV, peak B (C—O) at 286.9 eV, peak C (C=O) at 287.7 eV, and peak D (COOH) at 288.8 eV.

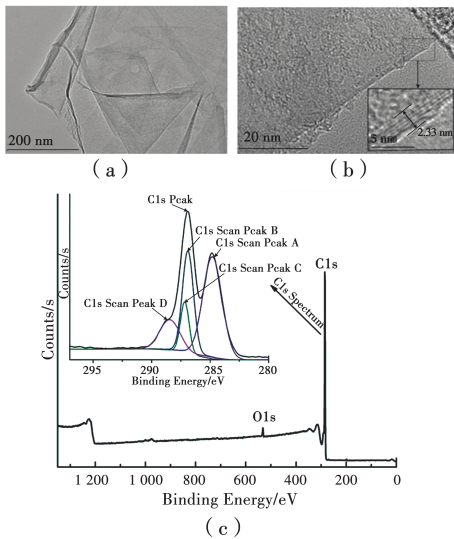


Fig. 3 (a)TEM, (b)HRTEM images and (c)XPS survey of graphene sheets

### 2.2 Specimen preparation

The preparation procedure is illustrated in Fig. 4. First, graphene and hexadecyl trimethyl ammonium bromide (CTAB) were dispersed into 50 mL deionized water and ultrasonicated for 10 min. Next, cement and lime were mixed and stirred, and slag and sand were added after 1 min of low speed stirring. Finally, the graphene dispersion was dropped into the CH mortar. Ramming was employed to make the particle distribution more uniform after mixing. The mixture was molded to different types of specimens

for testing and characterization.

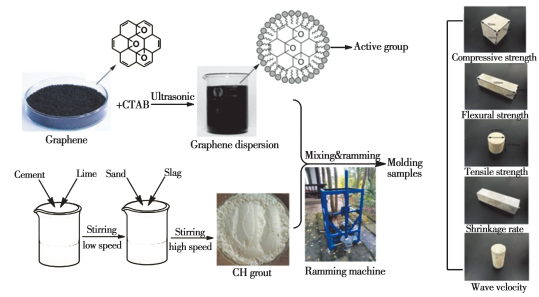


Fig. 4 Preparation of CH@G mortars

Table 2 presents the recipes for preparations of various CH and CH@G mortars. The weight percentages of the graphene sheets in the mortars were 0.01%, 0.03%, 0.05%, 0.07% and 0.10% of all raw materials (lime, cement, slag and sand). The water binder ratios of all specimens were 0.30. The size of the samples for compressive strength was 70.7 mm×70.7 mm×70.7 mm, and the flexural strength test samples were 40 mm×40 mm×160 mm. The Brazilian disc test was used to test the tensile strength of the samples, and the size of the samples was φ50 mm×100 mm.

Table 2 Recipes of CH and CH@G mortars

Samples	Lime/ %	Cement/ %	Sand/ %	Slag/ %	Graphene/ %
CH					0
CH@G-1					0.01
CH@G-2	22.2	11.1	26.7	40	0.03
CH@G-3					0.05
CH@G-4					0.07
CH@G-5					0.10

All samples for testing and characterization were cured in an environment (parameters: 8:00—20:00, 20 °C, RH 65%, 20:00—8:00, 15 °C, RH 75%) similar to that of the Leshan Giant Buddha area, and the parameters of the curing condition were controlled by a temperature and humidity curing box (BG/TH-100, Shanghai Bogong Equipment Co. Ltd.).

### 2.3 Experimental methods

#### 2.3.1 Shrinkage rate and ultrasonic wave velocity

The shrinkage rate of the specimens (40 mm×40 mm×160 mm) at different ages was measured

by an electronic micrometer with an accuracy of 0.001 mm. The ultrasonic wave velocity of the samples ( $\varphi=50$  mm, height=100 mm) at different ages was obtained by an RSM-SY5 (T) nonmetal acoustic detector.

### 2.3.2 Mechanical properties

Compressive strength, flexural strength and tensile strength were tested on a universal mechanical testing machine. The flexural strength of 40 mm  $\times$  40 mm  $\times$  160 mm samples was determined with a central-loading method, and then the compressive strength test was conducted after the flexural test on the remaining samples. The rate of loading was 2 mm/min. All test results were the average value of three replicate samples.

### 2.3.3 Characterization

The microstructure of all samples was examined by scanning electron microscope (Hitachi S-4800, Japan) and transmission electron microscope (Hillsboro, Tecnai G2 F20). Chemical state assignment was performed using X-ray photoelectron spectroscopy (Waltham, Thermal Scientific Escalab 250 Xi). Surface characterizations of specimens were obtained by FT-IR spectra analysis (Bruker, Tensor 27), Raman spectra analysis (France, LabRAM HR) and X-ray diffraction (Rigaku, D/max-2400).

## 3 Results and discussion

### 3.1 Shrinkage rate

The shrinkage rates of all samples are shown in Fig. 5. The shrinkage rate of the CH specimen increases rapidly during 0-7 d, and then slowly increases from 8 d to 14 d. Finally, the value remains almost constant after 15 d. The CH@G specimens show a tendency similar to that of the CH specimen, but all shrinkage rate values are lower than those of the CH specimen, indicating that the addition of graphene can enhance the volume stability of the CH@G specimens. When percentage of graphene added is 0.07 wt%, the specimen has the lowest shrinkage rate (0.39%) and the attenuation is 34.74% compared to the CH

specimen (0.59%).

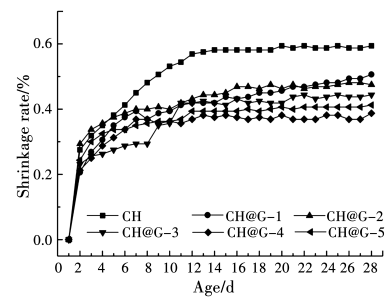


Fig. 5 Shrinkage rate of specimens at different ages

### 3.2 Ultrasonic wave velocity

Ultrasonic wave velocity tests were employed to reflect the degree of solidification of the samples<sup>[16]</sup>. As shown in Fig. 6, all specimen values first decrease and then increase. Finally, the value becomes stable. At 0 d, each sample has a high initial value due to the water filling in the pores. During 1-3 d, the water in the pores is absorbed by the cement and lime, and the wave velocity drops rapidly due to the loose and porous microstructure. At 4-14 d, the wave velocity of each specimen is simultaneously improved as the cement and lime solidify, and the velocity value increases as graphene is added. In the last period (15~28 d), the wave velocities become stable. At 28 d, the velocities of the CH@G specimens are higher than those of the CH specimen. The velocity of the CH@G-4 specimen is 1 670 m/s, which is the highest value among all the samples, and the increasement is 15.17% compared to the CH specimen.

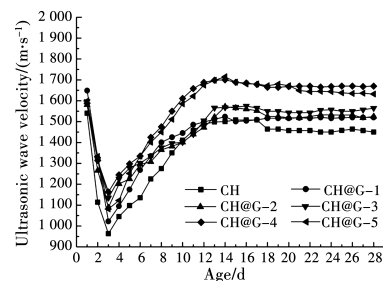


Fig. 6 Ultrasonic wave velocity of specimens at different ages

### 3.3 Mechanical properties

#### 3.3.1 Compressive strength

As shown in Fig. 7, the compressive strength of the CH specimen at 56 d is only 3.94 MPa. The

compressive strengths of the CH@G specimens increase with the addition of graphene, and the highest strength is obtained at 0.07 wt%. The strength completion degree is used to describe the hardening rate of each sample. The compressive strength value of each sample at 56 d is used as the reference value in the compressive strength completion degree curve<sup>[17]</sup>. The hardening rate gets faster in the CH@G specimens. The compressive strength completion degree of the CH and the CH@G specimens (1-5) at 7 d are 52.30%, 60.80%, 62.69%, 65.90%, 66.11% and 65.78%, respectively, suggesting that the addition of graphene could accelerate the hydration of the CH@G specimens in the early days.

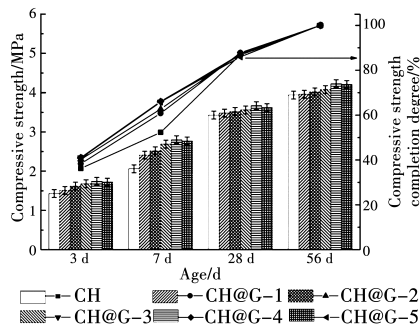


Fig. 7 Compressive strength of specimens at 3 d, 7 d, 28 d and 56 d

### 3.3.2 Flexural strength

The flexural strengths are shown in Fig. 8. The flexural strengths of the CH specimen are 0.89 MPa (3 d), 1.34 MPa (7 d), 1.60 MPa (28 d) and 1.85 MPa (56 d). With the addition of graphene, the flexural strength at 56 d increased for different degrees and the largest increment is 19.46% obtained in the CH@G-4 sample. The 56 d flexural strength values of each sample are used as the reference value in the flexural strength completion degree curve. The flexural strength completion degree curve shows a tendency similar to that of the compressive strength completion degree curve. The flexural strength completion degrees at 7 d are 72.40% (CH), 74.71% (CH@G-1), 75.22% (CH@G-2), 76.92% (CH@G-3), 76.94% (CH@G-4), and 76.33% (CH@G-5), indicating that the addition of graphene has the

potential to enhance the hydration reaction.

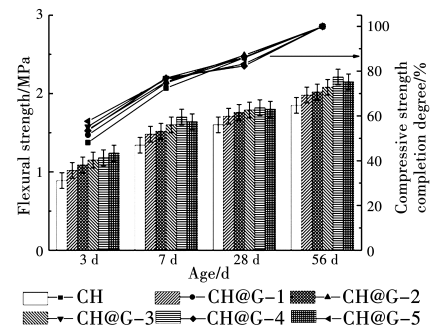


Fig. 8 Flexural strength of specimens at 3 d, 7 d, 28 d and 56 d

### 3.3.3 Tensile strength

As shown in Fig. 9, the tensile strength of the CH specimen at 3 d, 7 d, 28 d and 56 d are 0.13 MPa, 0.18 MPa, 0.24 MPa, and 0.31 MPa, respectively. The tensile strength of the CH@G specimens increases with the addition of graphene. The CH@G-4 sample exhibits the highest strength value (0.47 MPa), and the increment is 51.61%. The result shows that the addition of graphene to the CH@G specimens has a significant influence on the tensile strength. The 56 d tensile strength value of each sample is used as the reference value in the tensile strength completion degree curve. The tensile strength completion degree of the CH specimen at 7 d is 58.1%. With the addition of graphene, the tensile strength completion degrees of the CH@G specimens, which are 60.00%, 60.00%, 64.12%, 61.73% and 62.23%, change a little at each dosage of graphene (0.01%, 0.03%, 0.05%, 0.07% and 0.10%).

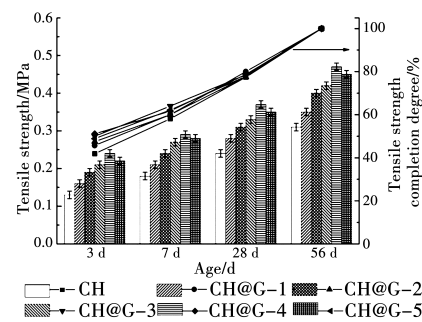


Fig. 9 Tensile strength of specimens at 3 d, 7 d, 28 d and 56 d

## 3.4 Products characteristics

### 3.4.1 FT-IR spectra

The FT-IR spectra of graphene, CH mortar

and CH@G mortars at 28 d are presented in Fig. 10. As shown in Fig. 10, a characteristic broad band that is responsible for hydroxyl stretching can be observed around  $3450\text{ cm}^{-1}$ . The  $\text{—COOH}$  carbonyl stretching at  $1730\text{ cm}^{-1}$  for graphene is very weak, likely because the absorption is slight and is obscured by the range band of  $\text{C=C}$  at  $1630\text{ cm}^{-1}$  [18-19]. The spectra of the CH mortar and the CH@G mortars have similar characteristic peaks such as  $3460\text{ cm}^{-1}$  ( $\text{—OH}$ ),  $1470\text{ cm}^{-1}$  ( $\text{O—C—O}$ ) and  $778\text{ cm}^{-1}$  ( $\text{O—C—O}$ ),  $950\text{ cm}^{-1}$  ( $\text{C—S—H}$ ) and  $510\text{ cm}^{-1}$  ( $\text{Si—O—Si}$ ). The results indicate that the addition of graphene has little influence on the composition of the products. However, the characteristic peaks of graphene can rarely be observed in the FT-IR spectra of the CH@G mortars. The Raman spectra are employed to further analyze the existence of graphene in the CH@G mortars.

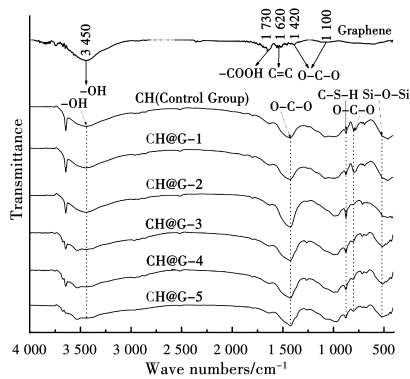


**Fig. 10 FT-IR spectra of graphene, CH mortar and CH@G mortars at 28 d**

### 3. 4. 2 Raman spectra

The Raman spectra of graphene, CH mortar and CH@G mortars at 28 d are shown in Fig. 11. The spectrum of graphene contains three peaks, namely D peak at  $1350\text{ cm}^{-1}$ , G peak at  $1582\text{ cm}^{-1}$  and 2D peak at  $2700\text{ cm}^{-1}$ . The D peak and 2D peak represent the high-frequency  $E_{2g}$  phonon at the center of the Brillouin zone, and the G peak corresponds to the breathing modes of six-atom rings [20]. The spectrum of the CH mortar has four characteristic peaks, including  $[\text{CO}_3]$  bending vibration,  $[\text{CO}_3]$  symmetric stretching vibration, C bending vibration and O bending vibration, and

similar characteristic peaks are observed in the spectra of the CH@G mortars. The results confirm that the addition of graphene has little influence on the composition of the products. A weakened peak at  $1550\text{ cm}^{-1}$ , the G peak of graphene, can be observed in the spectra of CH@G-2, CH@G-3, CH@G-4 and CH@G-5, and the intensity of this peak increased as the percentage of graphene added increased. It suggests that the graphene has been successfully added into the CH@G mortars.

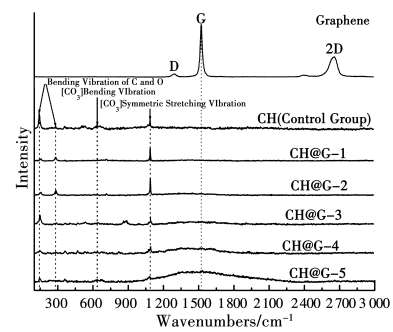


**Fig. 11 Raman spectra of graphene, CH mortar and CH@G mortars at 28 d**

### 3. 4. 3 XRD

XRD patterns of CH mortar, CH@G-2 mortar and CH@G-4 mortar curing at different ages are shown in Fig. 12. The specimens are mainly composed of  $\text{Ca(OH)}_2$ ,  $\text{CaCO}_3$ ,  $\text{SiO}_2$ , AFt and unhydrated  $\text{C}_3\text{S}$ , but C-S-H could not be indexed by XRD due to its amorphous property [21]. The peak intensity of unhydrated  $\text{C}_3\text{S}$  can be used to analyze the hydration rate of each sample. As shown in Fig. 12 (a), the peak intensity of unhydrated  $\text{C}_3\text{S}$  in the CH specimen at 1 d is a little higher than those specimens of CH@G-2 and CH@G-4, indicating that the hydration rate of the CH mortar is equivalent to that of the CH@G-2 and CH@G-4 mortars at the first period (0-1 d). From Fig. 12 (b), the peak intensity of unhydrated  $\text{C}_3\text{S}$  in the CH specimen at 3 d is much higher than those specimens of CH@G-2 and CH@G-4, and the peak shows a decreasing trend with the increasing contents of graphene. The results suggest that the hydration rate of the CH mortar is much slower than that of the CH@G-2 mortar and the CH@G-4 mortar at the second period (1-3 d). The hydration

rate of the CH mortar is slower than that of the CH@G-2 mortar and the CH@G-4 mortar at the third period (3-7 d), as shown in Fig. 12 (c). In the fourth period, the peak intensity of the unhydrated  $C_3S$  in the CH mortar is as great as those of the CH@G-2 mortar and the CH@G-4 mortar.

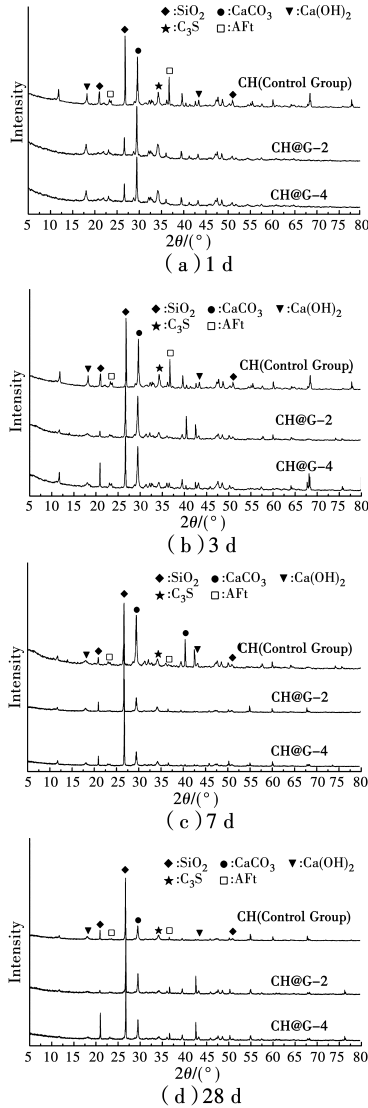


Fig. 12 XRD patterns of CH mortar, CH@G-2 mortar, and CH@G-4 mortar curing for (a) 1 d (b) 3 d (c) 7 d and (d) 28 d

The peak of  $Ca(OH)_2$  at  $18^\circ$  can be used to analyze the amount of  $Ca(OH)_2$  due to its good crystallinity<sup>[22]</sup>. The intensity of  $Ca(OH)_2$  in CH at 1 d is as high as that in the CH@G-2 and CH@G-4, meaning that the hydration rate of each sample is similar to that in first period. The intensity of  $Ca(OH)_2$  in the CH at 3 d is higher than that in CH@

G-2 and CH@G-4, indicating that the hydration rate of the CH@G specimens is quicker than that of the CH specimen. The trend shows a tendency similar to the change of  $C_3S$ . The results of XRD demonstrate that graphene could enhance the hydration of cement in the early days, leading to higher strength of the CH@G mortars.

### 3.5 Product morphology

As shown in Fig. 13 (a), the CH specimen is mainly the crystal aggregation of laminated  $Ca(OH)_2$  and fibrous C—S—H, and the whole microstructure is loose. Fig. 13 (b), (c) show the morphology of the CH@G-2 specimen and the CH@G-3 specimen, and the microstructure of the two specimens is similar to that of the CH specimen. As shown in Fig. 13 (d), a small amount of graphene sheets exist between particles, and the microstructure is still loose, indicating that the effect of the graphene is not significant at this content. From Fig. 13 (e), graphene sheets can be observed in the CH@G-4 specimen, and the microstructure of the CH@G-4 specimen is more uniform and dense compared with the CH specimen. As shown in Fig. 13 (f), more graphene sheets can be observed, but the graphene shows a tendency to agglomerate. It can be concluded that the effect of graphene in the CH@G-5 specimen is

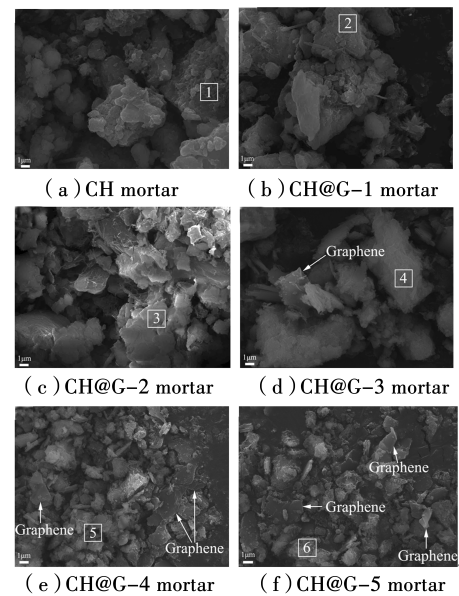


Fig. 13 SEM images of mortars at 28 d

not more remarkable than that of the CH@G-4 specimen. From the results of EDS (Table 3), the addition of graphene has no significant influence on the composition of the CH@G specimens, according to the

results of FT-IR, Raman and XRD. The results of SEM and EDS suggest that a sprinkling of graphene can control the shape and arrangement of the products in the CH@G specimens.

**Table 3** EDS data of marked area in SEM images

Sample	Element, Atomic/%							
	C	O	Mg	Al	Si	K	Ca	Fe
CH	21.23	58.37	1.04	3.66	8.85	0.85	4.12	1.88
CH@G-1	22.33	57.36	1.03	4.04	9.02	0.85	4.85	0.52
CH@G-2	22.52	57.01	0.98	4.12	9.11	0.69	4.98	0.59
CH@G-3	21.98	57.25	0.95	4.22	9.25	0.65	5.02	0.68
CH@G-4	21.38	57.02	0.98	4.31	9.29	0.63	5.12	1.27
CH@G-5	22.08	57.66	1.05	4.28	9.22	0.58	5.05	0.08

### 3.6 Mechanism analysis

According to the experimental results and the discussion above, the possible mechanism by which the addition of graphene influences the mechanical properties of CH mortar can be illustrated as follows (Fig. 14). In the hydration process, a complex reaction is carried out among  $C_2S$ ,  $C_3S$ ,  $C_3A$  and  $C_4AF$ . The products of hydration are AFt, AFm,  $Ca(OH)_2$  and C—S—H. The corresponding reactions are expressed by Eqs. (1)~(4).

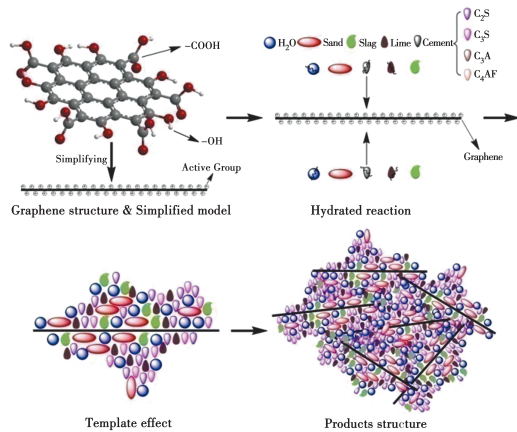
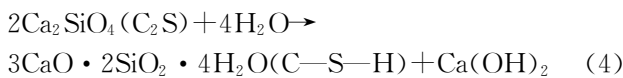
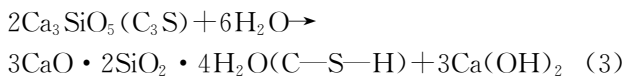
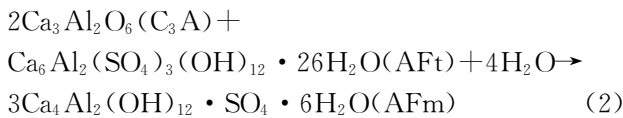
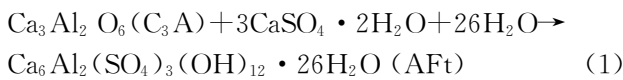


**Fig. 14** Mechanism by which graphene influences the CH@G mortars

Graphene sheets involve active groups ( $-OH$ ,  $-COOH$ , and  $-SO_3H$ ) after being functionalized by CTAB, and acid-based reactions take place between these active groups and  $Ca(OH)_2$ , leading to a strong covalent force on the interface between the graphene and the CH matrix<sup>[6]</sup>. The reaction sites and patterns are simultaneously controlled by the graphene, which is called the template effect<sup>[23]</sup>. The products of hydration grow forward from the surface of the graphene in the same direction, exhibit in an ordered way, and form a uniform and compacted microstructure. The resultant products improve the strength and volume stability of the CH@G mortars. Once the microstructure starts to crack or lose stability, they would disperse into the pores and cracks as filler to retard crack propagation.

## 4 Conclusion

Graphene is used to enhance the mechanical properties of CH@G mortars in this study. With the increase of graphene sheets, the mechanical properties of the CH@G mortars are enhanced. The specimen with the highest strength is found at 0.07 wt% level of graphene addition, where the compressive strength, flexural strength and tensile strength at 56 d are 4.21 MPa, 2.21 MPa and 0.47 MPa, respectively. FT-IR and Raman spectra show that the addition of graphene has little influence on the composition of the products, and from the XRD results, the graphene could enhance the hydration in the early days.

## Acknowledgements

The authors would like to acknowledge the financial support from the Sichuan Science and Technology Program (No. 2020YFS0391) and Key Research Project of China Railway Academy Co. Ltd. (No. 2019-KJ011-Z010-A2, No. 2020-KJ009-Z009-A2).

## References:

- [1] WEI J P, ZHU B L. Study on the sandstone weathering sensitivity caused by the changes of temperature and humidity [J]. *Advanced Materials Research*, 2011, 243-249: 645-649.
- [2] LI J H, LIU Z L, YU H, et al. The geological heritage of mount Emei in Sichuan Province and its geological significance [J]. *Advances in Earth Science*, 2015, 30(6): 691-699.
- [3] SINGH A P, MISHRA M, CHANDRA A, et al. Graphene oxide/ferrofluid/cement composites for electromagnetic interference shielding application [J]. *Nanotechnology*, 2011, 22(46): 465701.
- [4] PAN Z, HE L, QIU L, et al. Mechanical properties and microstructure of a graphene oxide-cement composite [J]. *Cement and Concrete Composites*, 2015, 58: 140-147.
- [5] DU H J, PANG S D. Enhancement of barrier properties of cement mortar with graphene nanoplatelet [J]. *Cement and Concrete Research*, 2015, 76: 10-19.
- [6] CAO M L, ZHANG H X, ZHANG C. Effect of graphene on mechanical properties of cement mortars [J]. *Journal of Central South University*, 2016, 23 (4): 919-925.
- [7] LIU H T, JIN J Z, YU Y J, et al. The mechanical properties and micro-structure of oil well cement enhanced by graphene oxide [J]. *Materials Science Forum*, 2018, 916: 200-204.
- [8] JIANG R S, WANG B M. Mechanical properties and microstructure of graphene-cement composites [J]. *Key Engineering Materials*, 2017, 748: 295-300.
- [9] LING X, WU J X, XU W G, et al. Probing the effect of molecular orientation on the intensity of chemical enhancement using graphene-enhanced Raman spectroscopy [J]. *Small*, 2012, 8(9): 1365-1372
- [10] ZHANG S, ZHANG X W, LIU X K, et al. Raman peak enhancement and shift of few-layer graphene induced by plasmonic coupling with silver nanoparticles [J]. *Applied Physics Letters*, 2014, 104(12): 121109.
- [11] PANG H, CHEN T, ZHANG G M, et al. An electrically conducting polymer/graphene composite with a very low percolation threshold [J]. *Materials Letters*, 2010, 64(20): 2226-2229.
- [12] BLANTER Y M, MARTIN I. Transport through normal-metal-graphene contacts [J]. *Physical Review B*, 2007, 76(15): 155433.
- [13] WALKER L S, MAROTTO V R, RAFIEE M A, et al. Toughening in graphene ceramic composites [J]. *ACS Nano*, 2011, 5(4): 3182-3190.
- [14] ALKHATEB H, ALOSTAZ A, CHENG A, et al. Materials genome for graphene-cement nanocomposites [J]. *Journal of Nanomechanics and Micromechanics*, 2013, 3(3): 67-77.
- [15] LV S, MA Y J, QIU C C, et al. Regulation of GO on cement hydration crystals and its toughening effect [J]. *Magazine of Concrete Research*, 2013, 65 (20): 1246-1254.
- [16] CARETTE J, STAQUET S. Monitoring the setting process of mortars by ultrasonic P and S-wave transmission velocity measurement [J]. *Construction and Building Materials*, 2015, 94: 196-208.
- [17] WANG N, CHEN W W, ZHANG J K, et al. Evolution of properties under realistic curing conditions of calcined ginger nut grouting mortars used in anchoring conservation of earthen sites [J]. *Journal of Cultural Heritage*, 2019, 40: 69-79.
- [18] QIAO Z, MAO J. Multifunctional poly (melamine-urea-formaldehyde)/graphene microcapsules with low infrared emissivity and high thermal conductivity [J]. *Materials Science and Engineering: B*, 2017, 226: 86-93.
- [19] QIAO Z, MAO J. Enhanced thermal properties with graphene oxide in the urea-formaldehyde microcapsules containing paraffin PCMs [J]. *Journal of Microencapsulation*, 2017, 34(1): 1-9.
- [20] FERRARI A C, BASKO D M. Raman spectroscopy as a versatile tool for studying the properties of graphene [J]. *Nature Nanotechnology*, 2013, 8(4): 235-246.
- [21] LUO K, LI J, LU Z Y, et al. Effect of nano-SiO<sub>2</sub> on early hydration of natural hydraulic lime [J]. *Construction and Building Materials*, 2019, 216: 119-127.
- [22] QIAO Z, SUN B, WANG F, et al. Age performance of Leshan Giant Buddha restoration material by metakaolin modified [J]. *Bulletin of the Chinese Ceramic Society*, 2020 39(2): 543-551.
- [23] LV S, MA Y J, QIU C C, et al. Effect of graphene oxide nanosheets of microstructure and mechanical properties of cement composites [J]. *Construction and Building Materials*, 2013, 49: 121-127.